LINEAR AND NON-LINEAR DYNAMIC ANALYSIS OF STOCKBRIDGE DAMPER

Nilson Barbieri, e-mail : nilson.barbieri@pucpr.br
Pontifícia Universidade Católica do Paraná – PUCPR
Universidade Tecnológica Federal do Paraná - UTFPR

Renato Barbieri, e-mail: renato.barbieri@pucpr.br
Pontifícia Universidade Católica do Paraná - PUCPR

Abstract. In this work a machine cam was used to investigate the linear and non-linear dynamical behavior of a asymmetric Stockbridge with excitation frequencies in the range of $5 \leq f \leq 17$ Hz. The loss factor and the Young modulus are estimated approximating experimental and numerical results with Genetic Algorithms (GAs). The two parameters depend on the excitation frequency and the base displacement. The forced response is obtained through the excitation generate by machine cam with five different profiles and the vibration signals are collected through accelerometers placed along the sample.

Keywords: Stockbrige damper; vibration; non-linear model.

1. INTRODUCTION

Wind-excited vibrations generated by vortex shedding are very common in high-voltage overhead transmission lines. Although such vibrations are rarely perceptible due to their low amplitudes (less than a conductor diameter), they are, however, extremely important since they may lead to conductor fatigue (Hagdorn *et al.*, 2002). These vibrations are usually caused by winds ranging in velocity from 1 to 10 m/s and can occur at frequencies from 3 to 150 Hz. In conventional transmission line systems, one or more dampers may be attached to a conductor in an effort to suppress aeolian vibrations.

The Stockbridge damper is presently the most common type of transmission-line damper. In general, a Stockbridge-type damper consists of two weights attached to the end of stranded cables, which are known as *messenger wires*. In this work the behavior of an asymmetric Stockbridge damper with four resonant response frequencies in the range $10 \leq f \leq 60$ Hz is analyzed.

Vecchiarelli, Currie and Havard (2000) introduced an iterative finite-difference scheme to predict the vertical, steady-state, monofrequent, aeolian vibration of a single conductor span with a Stockbridge-type damper attached. This numerical scheme is based on empirical models developed to represent the vortex-induced lift force from the wind as well as the forces of dissipation associated with the conductor self-damping and the damper. The scheme has the capability to account for more than one spatial mode of conductor vibration, travelling-wave effects, conductor flexural rigidity, and damper mass. A two-part numerical analysis is performed in which the "finite-difference scheme is applied to simulate aeolian vibrations of a typical conductor with and without a Stockbridge-type damper.

A detailed mathematical description of conductor motion is difficult due to the stranded construction of a conductor. An example of this problem is the study realized by Nawrocki and Labrosse (2000) where the cable is modeled using each individual wire model and all possible contacts are investigated. Although to get good results for static analysis this model was not applied for dynamic problems and the dynamic friction between the individual wires of the cable was also not studied.

In Stockbridge dampers, mechanical energy is dissipated in wire cables ("damper or messenger cables"). The damping mechanism is due to statical hysteresis resulting from Coulomb (dry) friction between the individual wires of the cable undergoing bending deformation. Systems with statical hysteresis can be modeled by means of Jenkin elements arranged in parallel, consisting of linear springs and Coulomb friction elements. The damper cable is a continuous system and damping takes place throughout the whole length of the cable, so that distributed Jenkin elements are used. Using such a model for the damper cables, the equations of motion can be formulated for a Stockbridge damper, and discretization of the damper cable leads to a system of nonlinear ordinary differential equations. In order to test this dynamical model of a Stockbridge the experimental impedance curves are compared with numeric results (Sauter and Hagdorn, 2002).

Verma (2002) uses masing model for modeling the nonlinear damping behavior of the damper cable of Stockbridge damper. Quasi-static behavior of cable was approximated by considering it as a linearly elastic Euler-Bernoulli beam. Model of damper cable was, then, transferred to the half of the Stockbridge damper body, considering it as symmetric, for getting the dynamic behavior of damper by determining its impedance. The impedance for different vibrational frequencies were computed. Results for model were then, verified by comparing them with the impedance obtained from experiments on real Stockbridge damper. It was found that the behavior of a damper cable could be reasonably described by using the masing model.

Markiewicz (1995) analyzed the optimum dynamic characteristics of Stockbridge dampers for dead-end spans. The analysis showed that the optimum damper impedance required for such spans (called dead-end spans) differs significantly from the optimum impedance of the standard damper and also showed how the efficiency of a standard damper used in such spans may be improved by its proper location on a cable.

Wang *et al.* (1997) analyzed the free vibration of a transmission line conductor equipped with a number of Stockbridge dampers modeled by a differential equation of motion of a tensioned beam acted on by concentrated frequency dependent forces and an exact solution is obtained using integral transformation.

Espíndola and Silva Neto (2001) using a three-degree of freedom model to modeling the Stockbridge damper, showed the viscoelastic behavior of the flexural stiffness. This model is similar to model used by Sauter and Hagdorn (2002) and Verma (2002).

Zhu and Meguid (2006, 2007a e 2007b) analyzed the behavior of cables considering curved beam models. Due to difficulties in modeling the hysteretic damping it was used the standard Rayleigh damping. The numerical and experimental results presented good approximation.

López and Venegas (2001) analyzed the dynamic behavior of stockbridges through dynamic and fatigue tests, and showed the damping ratio decreases linearly with the amplitude of excitation motion.

In this work the physical parameters are adjusted through the comparison between numerical and experimental results. The numerical models are obtained using Finite Element Method. The experimental results are obtained using a cam machine with five different eccentricities. In this way the motion amplitude of the excitation is maintained constant. The experimental results are compared with linear and nonlinear numerical results. The nonlinear system contains nonlinear stiffness and damping elements. The dynamic responses of linear and nonlinear systems are also compared with experimental results (impedance curves) obtained through conventional testing using eletromechanical shaker to excite the system.

2. MATHEMATICAL MODELS

In this section are shown the mathematical models of the Stockbridge damper system.

2.1. Messenger Wire Model

The messenger wire is modeled using the Euler-Bernoulli beam finite element. In this element the transversal displacement is interpolated using the well-known *Hermitian interpolation polynomials* with C^1 continuity and the degrees of freedom (d.o.f) in each node are the transversal displacement and the rotation, $\{v,\theta\}$. The dynamic equation for this element can be written in the following form:

$$\frac{\rho AL}{420}\begin{bmatrix} 156 & 22L & 54 & -13L \\ & 4L^2 & 13L & -3L^2 \\ & & 156 & -22L \\ \text{sim.} & & & 4L^2 \end{bmatrix}\begin{Bmatrix} \ddot{v}_1 \\ \ddot{\theta}_1 \\ \ddot{v}_2 \\ \ddot{\theta}_2 \end{Bmatrix} + \frac{EI}{L^3}\begin{bmatrix} 12 & 6L & -12 & 6L \\ & 4L^2 & -6L & 2L^2 \\ & & 12 & -6L \\ \text{sim.} & & & 4L^2 \end{bmatrix}\begin{Bmatrix} v_1 \\ \theta_1 \\ v_2 \\ \theta_2 \end{Bmatrix} = -\frac{\rho AL}{12}\begin{Bmatrix} 6 \\ L \\ 6 \\ -L \end{Bmatrix}\ddot{y}_0 \qquad (1)$$

where ρA is the linear density of cable, L is the finite element length, EI is a cable flexural (bending) stiffness and $\ddot{y}_0$ is the base acceleration excitation (shaker).

To take in consideration the cable *hysteretic damping* in equation (1) it is sufficient to consider the flexural stiffness as

$$EI = EI_0 (1 + \beta i) \qquad (2)$$

where β is the *hysteretic damping constant* and $i = \sqrt{-1}$.

2.2. Damper Mass Model

The suspended masses of the shock absorber (Stockbridge) are modeled with rigid body plane motion hypothesis and the admissible displacements are shown in the Fig. 1.

After the assembly of all the elements of the messenger wire, each one of the Stockbridge damper weights contributes with two terms for the dynamical equilibrium. The first contribution is in the mass matrix (inertia force)

$$[M_S]\{\ddot{q}_n\} = \begin{bmatrix} m & m\overline{x} \\ m\overline{x} & I_n \end{bmatrix} \begin{Bmatrix} \ddot{v}_n \\ \ddot{\theta}_n \end{Bmatrix} \tag{3}$$

and another parcel is in the vector force due to base acceleration

$$\{f_s\} = -\begin{Bmatrix} m \\ m\overline{x} \end{Bmatrix} \ddot{y}_0 \tag{4}$$

where m is the mass of Stockbridge damper weight, $\overline{x}$ is the center of mass coordinate and I_n is the inertia moment with reference fixed in node n.

These two terms are obtained using the first variation of the kinetic energy (Hamilton Principles) and the rigid body plane motion hypothesis for suspended Stockbridge damper weight modeling. With the convention defined in the Fig.1, the kinetic energy of each one of the Stockbridge damper weights can be written taking as reference the node n (the node of the finite element mesh connected to the messenger wire). This expression is:

$$T = \frac{1}{2} m\dot{r}_n \bullet \dot{r}_n + \dot{r}_n \bullet [\omega \times m\overline{x}] + \frac{1}{2} \omega \bullet \int_m \rho_n \times [\omega \times \rho_n] dm \tag{5}$$

where $\dot{r}_n$ is the velocity of node n, ω is the damper weight angular velocity and ρ_n is the particle position of dm mass with origin fixed in node n.

Taking in consideration the hypotheses of rigid body plane motion, $\omega = \dot{\theta}_n k$, and symmetry in y, ($\overline{y} = 0$), the expression for kinetic energy of damper weight can be rewrite after integration as:

$$T = \frac{1}{2} m [\dot{u}_n^2 + \dot{v}_n^2 + 2\dot{y}_0\dot{v}_n + \dot{y}_0^2] + \overline{x}m[\dot{\theta}_n\dot{v}_n + \dot{\theta}_n\dot{y}_0] + \frac{1}{2}I_n\dot{\theta}_n^2 \tag{6}$$

The variation of T can be write as $\delta T = \frac{\partial T}{\partial \dot{u}_n}\delta\dot{u}_n + \frac{\partial T}{\partial \dot{v}_n}\delta\dot{v}_n + \frac{\partial T}{\partial \dot{\theta}_n}\delta\dot{\theta}_n$. Integrating by parts the terms in $\delta\dot{v}_n$ and

$\delta\dot{\theta}_n$ and neglecting the boundary terms results the equations (3) and (4).
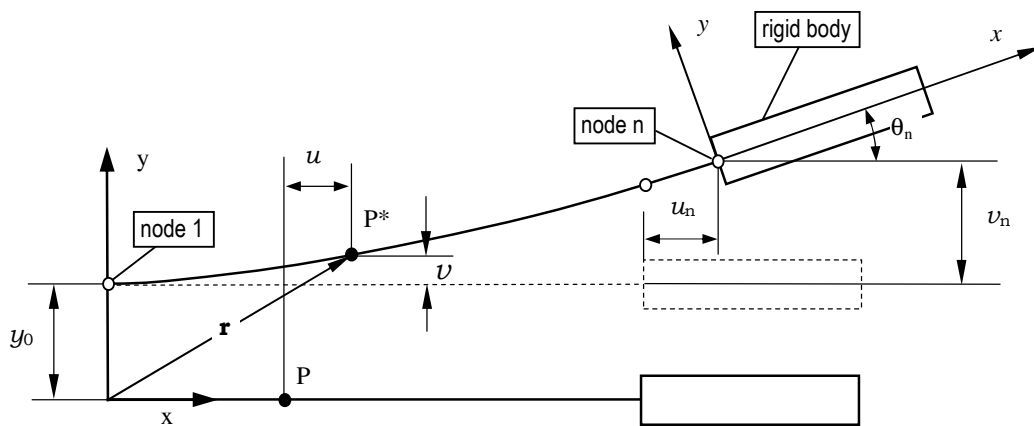
Figure 1 – References and admissible displacements.

2.3. Finite Element System of Equations

The Stockbridge discretized dynamical equilibrium equations is obtained after assembling all finite elements and can be written in the conventional way as

$$[M]\{\ddot{q}\} + [K]\{q\} = \{f_o\}\ddot{y}_o(t) \tag{7}$$

where [M] and [K] are the mass and stiffness matrices and $\{f_0\}$ is the force vector. The components of vector $\{q\}$ are the finite element node displacements and rotations, v and θ; and $\ddot{y}_0$ is the acceleration in node 1 (base shaker acceleration).

Admitting the base excitation as harmonic, $\ddot{y}_0(t) = |\ddot{y}_0|e^{i\omega t}$, the solution q(t) is of the form $\mathbf{q}(t) = \mathbf{q}_0\,e^{i\omega t}$. Substitution this assumed form of solution into the equation of motion (7) yields:

$$\left[-\omega^2[M] + [K]\right]\{q_o\} = |\ddot{y}_o|\{f_o\} \tag{8}$$

The amplitude of the displacement vector is calculated solving the Equation (8) for each frequency ω and the amplitude of the acceleration vector is easily calculated with the product $\omega^2\{q_o\}$.

2.4. The nonlinear formulation (Siller, 2004)

The parameter estimation of the nonlinear system can be made by approximating the numeric and experimental FRF curves. The analysis can be exemplified by considering the equation of motion of a simple oscillator subjected to a harmonic excitation (Kerschen et al., 2006; Siller, 2004) (Harmonic Balance Method):

$$m\ddot{y} + \tilde{g}(\dot{y}, y) = f\sin\omega t \tag{9}$$

where $\tilde{g}(\dot{y}, y)$ encloses all the restoring forces, assumed to be a nonlinear function of velocity and displacement $(\dot{y}, y)$ of the mass m.

If the response is sufficiently close to a pure sinusoidal, and provided that little energy is leaked to frequencies other than the fundamental, then it is reasonable to assume that the nonlinear function $\tilde{g}(\dot{y}, y)$ is also of a periodically-oscillating nature. It is possible to find a linearized coefficient $\tilde{v}(\dot{y}, y)$ which provides the best average of the true restoring force. This coefficient acts on the fundamental harmonic of the nonlinear response ($\tilde{Y}^{1st}$) for a single load-cycle in such a way that:

$$\tilde{g}(\dot{y}, y) \approx \tilde{v}(\dot{y}, y).y \quad \text{for } y \approx \tilde{Y}^{1st}\sin(\omega t + \theta) = \tilde{Y}^{1st}\sin(\tau) \tag{10}$$

In order to find the nonlinear coefficient $\tilde{v}(\dot{y}, y)$, the restoring force $\tilde{g}(\dot{y}, y)$ is expanded around y via a Fourier series, neglecting all the higher-order terms:

$$\tilde{g}(\dot{y}, y) \approx \tilde{v}(\dot{y}, y).y = \sigma_a^{1st}y + \sigma_b^{1st}y + \underbrace{\sigma_c^{2nd}y + \sigma_d^{2nd}y + ...}_{\text{neglected \quad terms}} \tag{11}$$

where the σ functions are given by:

$$\sigma_a^{1st} = \frac{1}{\pi\tilde{Y}^{1st}}\int_0^{2\pi}\tilde{g}(\tilde{Y}^{1st}\text{sen}\tau, \omega\tilde{Y}^{1st}\cos\tau)\sin\tau d\tau \tag{12}$$

$$\sigma_b^{1st} = \frac{1}{\pi\tilde{Y}^{1st}}\int_0^{2\pi}\tilde{g}(\tilde{Y}^{1st}\text{sen}\tau, \omega\tilde{Y}^{1st}\cos\tau)\cos\tau d\tau \tag{13}$$

So the nonlinear coefficient $\tilde{v}(\dot{y}, y)$ is uniquely defined by

$$\tilde{v}(\dot{y}, y) = \sigma_a^{1st} + \sigma_b^{1st} \tag{14}$$

The mathematical model of a cubic stiffness element can be expressed as:

$$\tilde{g}(\dot{y}, y) = ky + \beta y^3 \tag{15}$$

where the coefficient k represents the linear component of the spring, while the coefficient β accounts for the nonlinear effects due to the term y^3. Introducing (15) into (12) and (13), and dropping the superscript [1st] for sake of clarity, whe have:

$$\sigma_a = \frac{1}{\pi \tilde{Y}} \int_0^{2\pi} (ky + \beta y^3) \operatorname{sen}\tau d\tau \tag{16}$$

$$\sigma_b = 2\sin(\pi)\cos(\pi) = 0 \tag{17}$$

Introducing (16) and (17) into (14) and developing further:

$$\tilde{v}(y, \dot{y}) = \frac{k}{\pi}(\pi) + \frac{\beta \tilde{Y}^2}{\pi}\left(\frac{3}{4}\pi\right) \tag{18}$$

and we finally arrive to the first-order representation of a cubic stiffness element:

$$\tilde{v}(y, \dot{y}) = k + \frac{3\beta \tilde{Y}^2}{4} \tag{19}$$

where the second term in the right side of (19) represents the nonlinear part of the coefficient.

The nonlinear friction damping can be obtained using the similar approach to the cubic stiffness development. The nonlinear restoring force becomes:

$$\tilde{g}(\dot{y}, y) \approx \tilde{v}_c(\dot{y}, y).y \tag{20}$$

After applying the describing function formulation, the linearized coefficient $\tilde{v}_c(\dot{z}, z)$ is found to be:

$$\tilde{v}_c(\dot{y}, y) = i\omega c + i\frac{4\gamma}{\pi \tilde{Y}} \tag{21}$$

Expanding the idea of the simple oscillator introduced in (9) to an MDOF system, we have:

$$[M]\{\ddot{y}\} + \{\tilde{G}(\dot{y}, y)\} = \{F\}e^{i\omega t} \tag{22}$$

where $[M]$ is the mass matrix; $\{\ddot{y}\}$, $\{\dot{y}\}$ and $\{y\}$ are the acceleration, velocity and displacement vectors (respectively), and $\{F\}$ is a harmonic excitation vector operating at frequency ω.

For additive nonlinearities it is possible to expand the nonlinear vector into individual nonlinear restoring forces, as follows:

$$\{\tilde{G}(\dot{y}, y)\} = \begin{Bmatrix} \tilde{g}_{11} + \tilde{g}_{12} + \tilde{g}_{13} + \ldots\ldots + \tilde{g}_{1N} \\ \tilde{g}_{21} + \tilde{g}_{22} + \tilde{g}_{23} + \ldots\ldots + \tilde{g}_{2N} \\ \tilde{g}_{31} + \tilde{g}_{32} + \tilde{g}_{33} + \ldots\ldots + \tilde{g}_{3N} \\ . \\ . \\ . \\ \tilde{g}_{N1} + \tilde{g}_{N2} + \tilde{g}_{N3} + \ldots\ldots + \tilde{g}_{NN} \end{Bmatrix} \tag{23}$$

where N is the size of the system (in DOFs). Each nonlinear function $\tilde{g}_{ij}$ represents a restoring force acting between DOFs i and j, while terms with repeated indexes $\tilde{g}_{ii}$ represent a restoring force between DOF i and the ground.

Introducing the newly re-defined nonlinear coefficients into (21), a matrix of nonlinear coefficients is formed:

$$\{\tilde{G}(\dot{y}, y)\} = [\tilde{v}]\{\tilde{Y}\} \tag{24}$$

The equation motion of a general nonlinear system subjected to harmonic excitation can be described by the following nonlinear ordinary differential equation:

$$[M]\{\ddot{y}\} + [C]\{\dot{y}\} + i[D]\{y\} + [K]\{y\} + \{\tilde{G}(\dot{y}, y)\} = \{F\}e^{i\omega t} \tag{25}$$

where $[M]$, $[C]$, $[D]$ and $[K]$ are the mass, viscous damping, hysteretic damping and stiffness matrices (respectively) of the underlying linear system;; $\{\ddot{y}\}$, $\{\dot{y}\}$ and $\{y\}$ are the acceleration, velocity and displacement vectors, and $\{F\}$ is a harmonic excitation vector operating at frequency ω.

The nonlinear component of the system is represented by the nonlinear vector $\{\tilde{G}\}$, which is a function of all displacements and velocities in the general case.

Considering harmonic response $\{y(t)\} = \{\tilde{Y}\}e^{i\omega t}$, where $\{\tilde{Y}\} = \{|\tilde{Y}|e^{i\theta}\}$ is a nonlinear complex vector allowing it to accommodate phase, the equation of motion is further reduced to:

$$\left(-\omega^2[M] + i\omega[C] + i[D] + [K]\right)\{\tilde{Y}\} + \{\tilde{G}(\omega, \tilde{Y})\} = \{F\} \tag{26}$$

The linear receptance can be defined as:

$$[\alpha] = \left(-\omega^2[M] + i\omega[C] + i[D] + [K]\right)^{-1} \tag{27}$$

and its inverse , $[\Lambda] = [\alpha]^{-1}$, as:

$$[\Lambda] = -\omega^2[M] + i\omega[C] + i[D] + [K] \tag{28}$$

Introducing (24) and (28) into (26), we have:

$$([\Lambda] + [\tilde{v}])\{\tilde{Y}\} = \{F\} \tag{29}$$

leading to the final compact representation of the nonlinear function:

$$[\tilde{\Lambda}]\{\tilde{Y}\} = \{F\}, \text{ where: } [\tilde{\Lambda}] = [\Lambda] + [\tilde{v}] \tag{30}$$

$[\tilde{\Lambda}]$ is a composite matrix, enclosing linear and nonlinear coefficients, and it is formulated for the current state [$\dot{y}$, y , ω]. It can be considered to be the system matrix. Obtaining the roots of the determinant of $[\tilde{\Lambda}]$ yields the frequency-dependent nonlinear natural frequencies and damping ratios. The system response $\{\tilde{Y}\}$ can be obtained solving (30).

The solution of (30) can be used to adjustment and/or updated parameters in numerical models obtained by the Finite Element Method by comparing numerical and experimental results (Grafe, 1998). We have obtained satisfactory results using the method of genetic algorithms (Chang, 2006) to make the approximation of the numeric and experimental values.

3. RESULTS

Figure 1 show the schematic representation of the machine cam used to experimental tests of the stockbridge with controlled oscillation (displacement). Although the full stockbridge is represent in the analysis were considered only the half sample. The experimental data are obtained through three accelerometers placed in the half sample. One accelerometer was placed in the center position and other in the extremity of the messenger wire. The third accelerometer (reference) was placed in the connecting rod.
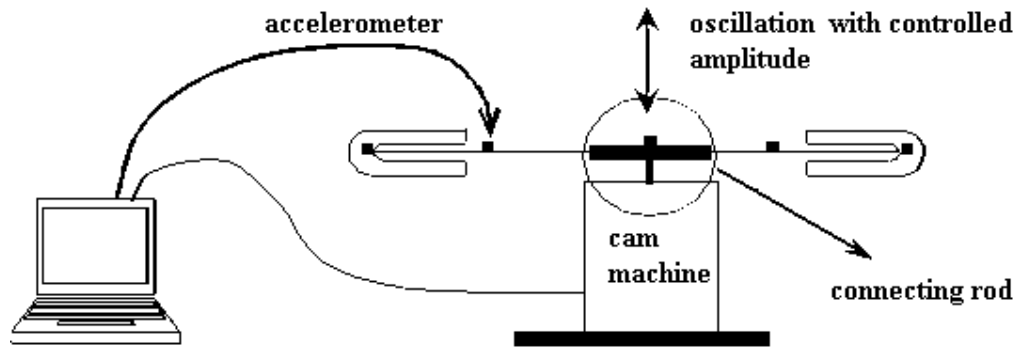
Figure 1 – Schematic cam machine.
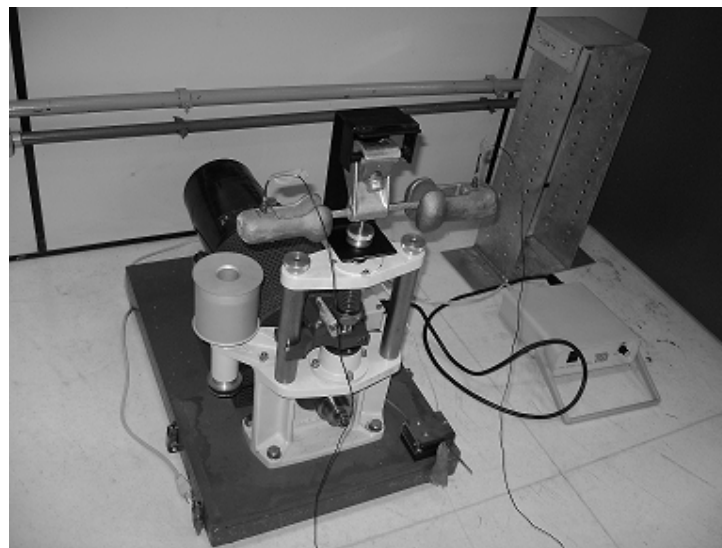
Figure 2 – Cam machine with stockbridge coupled.

Figure 2 show the cam machine with stockbrige coupled and two accelerometers positioned.

Five different cams with eccentricities of 0.25, 0.5, 0.75, 1.25, 1.5 mm were used. The tests were conduced varying the excitation frequency between 5 and 17 Hz with increments of 0.25 Hz. This frequency range was used due to the mechanical limitation of the excitation system. Figure 3 and 4 show the show the experimental curves of the acceleration ratio (non-dimensional parameter) Paa (acceleration of reference sensor / acceleration of the accelerometer in the cable) obtained to the accelerometer placed in the center (accelerometer 1) and to the accelerometer placed in the extremity (accelerometer 2) of the messenger wire. It can be noticed that the natural frequency changes with the motion amplitude. The frequency variation is inversely proportional to the motion amplitude. Figure 5(a) and 5(b) show the variation of the natural frequency and the damping ratio (adjusted to a linear system) with the amplitude of the base excitation. It can be noted that parameters, natural frequency and damping ratio, vary inversely with the increase of the amplitude of the base excitation. López and Venegas (2001) found slightly different results in experimental tests.
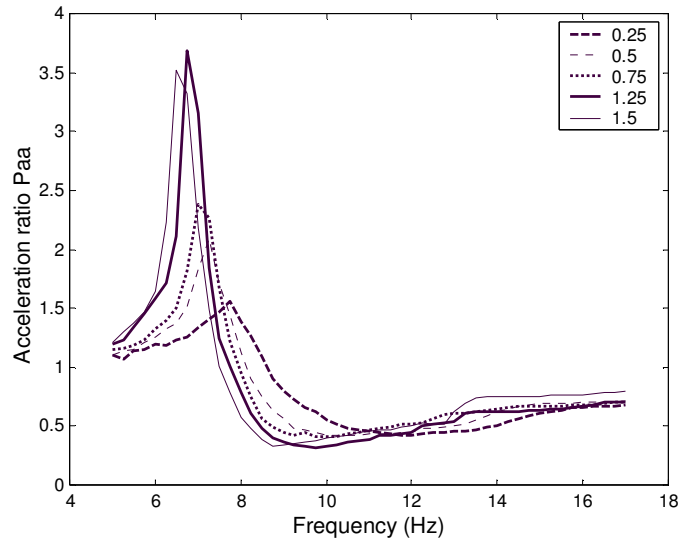
Figure 3 - Acceleration ratio curves of accelerometer 1.
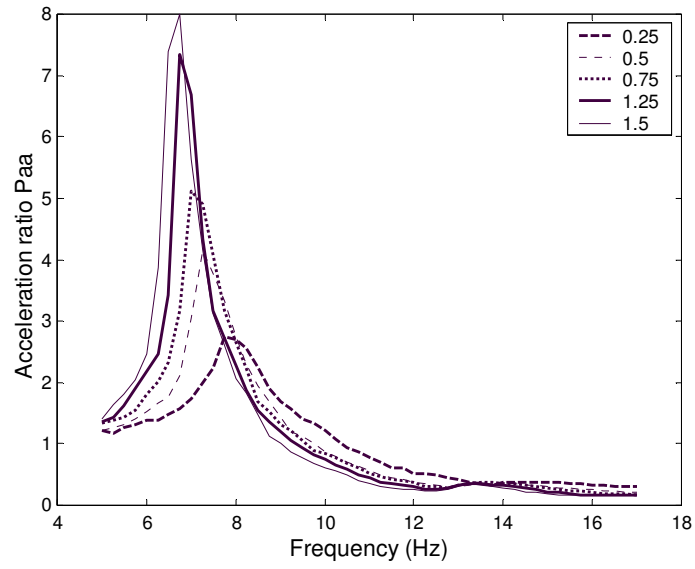
Figure 4 - Acceleration ratio curves of accelerometer 2.

Damping ratio

Accelerometer 1
Accelerometer 2

Frequency (Hz)

Displacement (mm)
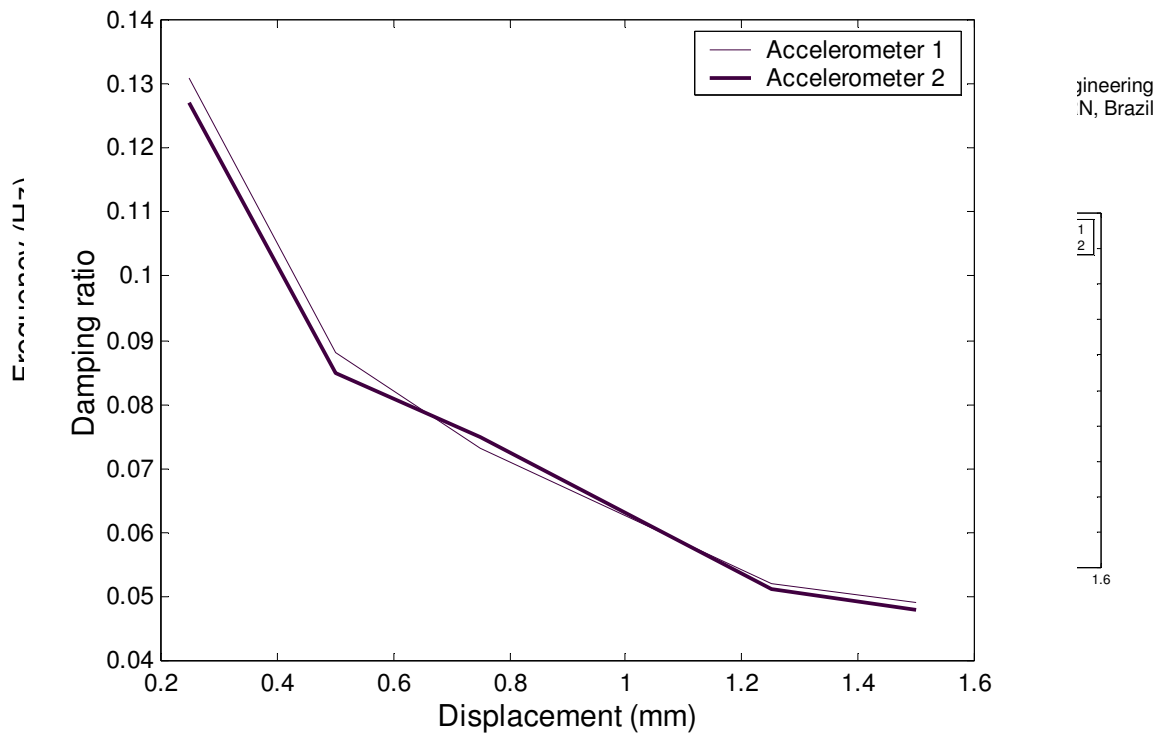
The linear and nonlinear parameters used in the numerical models were adjusted considering five different cam profiles. The results are shown in Table 1. The linear parameters adjusted are the Young modulus E and the loss factor η. The complex Young modulus is:

$$E_t = E(1 + i\eta)$$

where η is the loss factor. To simulate the hysteretic damping of the system it was considered $\eta = \eta_i / \omega$ (frequency dependent parameter). For the nonlinear system were adjusted these two parameters and the other nonlinear parameters of stiffness (β_1 and β_2) and damping (γ_1 and γ_2) described in (11) and (13). Using the procedure described by Siller (2004) and only considered the principal terms of the nonlinear stiffness and damping matrixes (main diagonal). The error column (Table 1) represent the sum of the absolute errors (difference between the linear and nonlinear FRF) obtained for a limited range of frequencies (approximately 2 Hz in the resonance region) divided by the number of points.

Table1 – Parameters adjusted for the linear and nonlinear systems.

Eccentricity (mm)		Absolute error	EI [Nm^2]	η_i	β_1 [N/m^3]	β_2 [N/m^3]	γ_1 [N]	γ_2 [N]
0.25	linear	0.589	1.90	9.82				
	nonlinear	0.600	1.98	11.46	-7.9e9	-0.0036	-0.0264	-0.0502
0.5	linear	0.454	1.74	6.21				
	nonlinear	0.480	1.69	7.68	-9.59e8	-0.0308	-0.0416	-0.0964
0.75	linear	0.496	1.65	4.40				
	nonlinear	0.464	1.67	6.57	-4.59e7	-0.0077	-0.0445	-0.0084
1.25	linear	0.568	1.52	2.94				
	nonlinear	0.569	1.54	3.72	-1.67e8	-0.0182	-0.0490	-0.0537
1.5	linear	0.828	1.43	2.56				
	nonlinear	0.797	1.08	11.24	-5.20e8	-0.1601	-0.0147	-0.0996

Figure 6(a) shows the reference base displacement curve obtained in a conventional testing using eletromechanical shaker for excitation. It can be noted that the base displacement variation with the frequency. As input for the mathematical system we considered the real acceleration measured at stockbridge. Figure 6(b) shows the acceleration curve of the base as a function of excitation frequency.

(a)

(b)
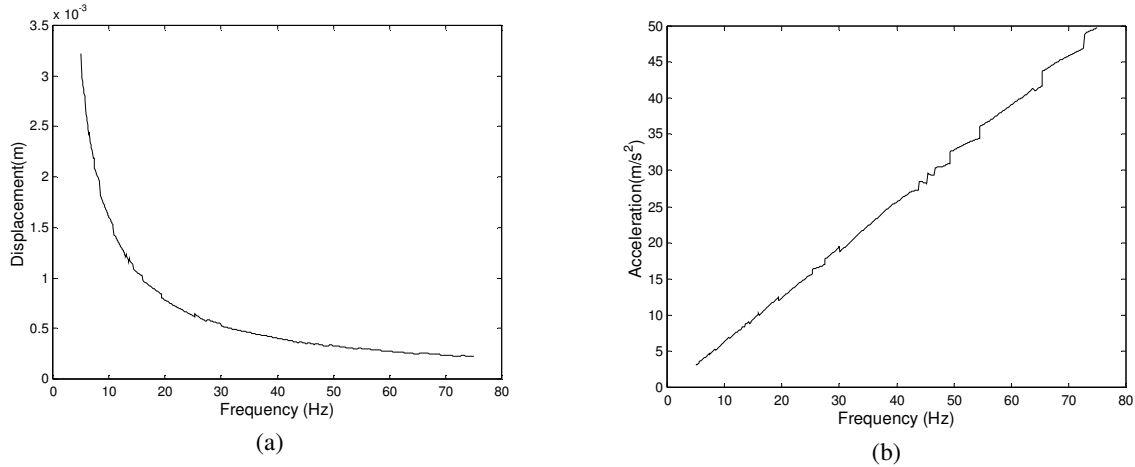
Figure 6 –Base displacement and acceleration.

According to the results shown in Table 1 we tried to adjust curves to the EI (bending stiffness) and NI (loss factor) (Figures 7(a) and 7(b)) due to the displacement of the base. These curves serve as reference for the parameters to be adjusted to a stockbridge tested in an electromechanical shaker with a displacement of the base.

(a)

(b)
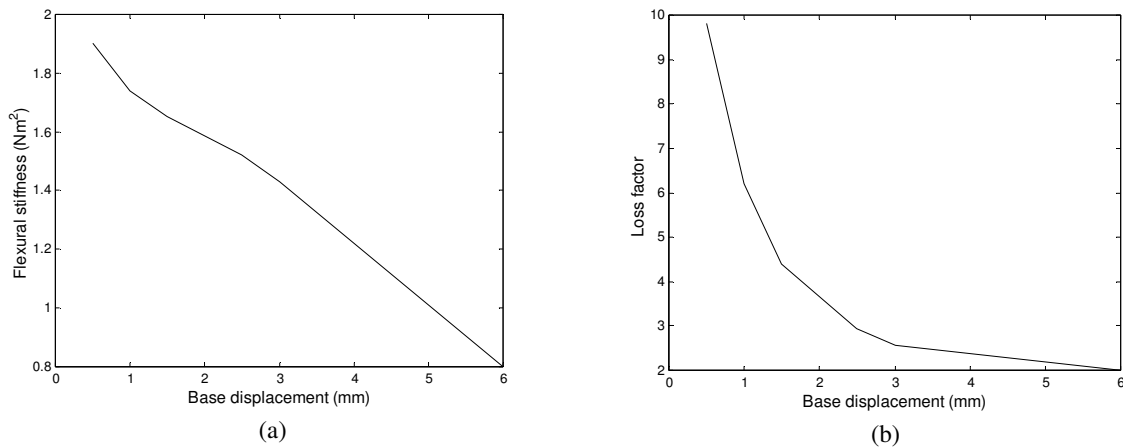
Figure 7 – Curve of the flexural stiffness and loss factor versus base displacement.

Finally, Fig. 8 shows the experimental and adjusted curves of cable acceleration. The curves presents good agreement for f<= 10 Hz (region of the first vibration mode). As the frequency testing is lower than 17 Hz, it is not possible to relate the curve results for f> 17 Hz.
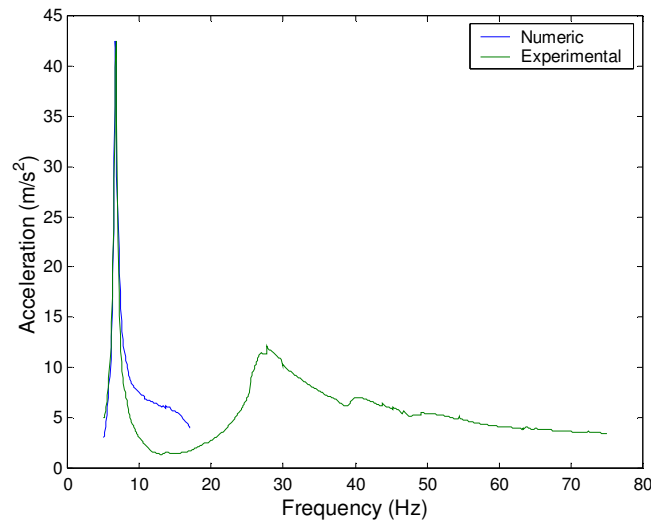
Figure 8 – Cable acceleration.

4. CONCLUSIONS

The results showed that the natural frequency of the system varies with the amplitude of the excitation motion, ie, as higher the amplitude of motion as lower is the natural frequency. The same behavior was verified for the damping ratio of the system, ie, as higher the amplitude of motion as lower is the damping ratio.

In the fit of parameters of a linear system, it was verified that the real and imaginary parts of the complex Young modulus decreases with increasing the amplitude of motion.

For the frequencies range $5 \le f \le 17$ Hz and the motion displacement minor than 1.5 mm the response of the system with nonlinear parameters did not show improvements in relation to the response of the linear system.

As the test was done with a full stockbridge, it is possible that the smaller cable and smaller mass have influenced the results. The mathematical model was based on only half model of stockbridge containing larger mass.

Since the tests were performed with constant amplitude of base motion it was possible to fit single value of the parameters according to the amplitude of motion. When the tests are conduced using electromechanical shaker the motion amplitude is varied according to the excitation frequency. In this case the fitted parameters are frequency dependent .

5. ACKNOWLEDGEMENTS

6. REFERENCES

Chang, W.-D., 2006, "An improved real-coded genetic algorithm for parameters estimation of nonlinear systems", Mech. Syst. Signal Proc., Vol. 20, pp. 236–246.

Espíndola, J. J. and Silva Neto, J. M., 2001, "Identification of Flexural Stiffness Parameters of Beams", J. Braz. Soc. Mech. Sci., Vol. 23, pp. 217-225.

Grafe, H., 1998, "Model updating of large structural dynamics models using measured response functions", PhD Thesis, Imperial College London/ University of London. 184p.

Hagedorn, P., Mitra, N., Hadulla, T., 2002, "Vortex–excited vibrations in bundled conductors: a mathematical model", Journal of Fluids and Structures, Vol. 16, pp. 843–854 .

Kerschen, G., Worden, K., Vakakis, A. F., Golinval, J.C., 2006, " Past, present and future of nonlinear system identification in structural dynamics". Mechanical Systems and Signal Processing, Vol. 20, pp. 505–592.

López, A. L., Venegas, J. C., 2001, "Endurance of dampers for electric conductors", International Journal of Fatigue , Vol. 23, pp. 21-28

Markiewicz, M., 1995, "Optimum dynamic characteristics of Stockbridge dampers for dead-end spans", Journal of Sound and Vibration, vol. 188, pp.243-256

Nawrocki, A., Labrosse, M., 2000, "A finite element model for simple straight wire rope strands", Computers and Structures , Vol. 77, pp. 345-359

Sauter, D., Hagedorn, P., 2002, "On the hysteresis of wire cables in Stockbridge dampers", International Journal of Non-Linear Mechanics, Vol. 37, pp. 1453-1459.

Siller, H. R. E., 2004, "Non-Linear Modal Analysis Methods for Engineering Structures", PHd Thesis. Imperial College London/University of London. 242 p.

Vecchiarelli, J., Currie I. G., Havards, D. G., 2000, "Computational analysis of aeolian conductor vibration with a Stockbridge-type damper", Journal of Fluids and Structures, Vol. 14, pp. 489-509

Verma, H., 2002, "The Stockbridge damper as a continuous hysteric system in single overhead transmission lines", Master Dissertation, Indian Institute of Technology Bombay, 81p..

Wang, H. Q., Miao, J. C., Luo, J. H., Huang, F. , Wang, L. G., 1997, "The free vibration of long-span transmission line conductors with dampers", Journal of Sound and Vibration , Vol. 208, pp. 501-516.

Zhu, Z. H., Meguid, S. A., 2006, "Elastodynamic analysis of low tension cables using a new curved beam element". International Journal of Solids and Structures, Vol. 43, pp. 1490–1504

Zhu, Z. H., Meguid, S. A., 2007a, " Modeling and simulation of aerial refueling by finite element method". International Journal of Solids and Structures, Vol. 44, pp. 8057-8073

Zhu, Z. H., Meguid, S. A., 2007b, "Nonlinear FE-based investigation of flexural damping of slacking wire cables". International Journal of Solids and Structures, Vol. 44, pp.5122-5132

7. RESPONSIBILITY NOTICE

The authors are the only responsible for the printed material included in this paper.